Investigation of δ-ferrite content in weld metal of modified 9Cr–1Mo electrodes using thermodynamic modelling and quenching experiments

S. S. Mahlalela[1], P. G. H. Pistorius[2]

SAIW Centre for Welding Engineering, Department of Materials Science and Metallurgical Engineering, University of Pretoria, Gauteng, South Africa.

Email: [1]sibusiso.mahlalela@up.ac.za [2]pieter.pistorius@up.ac.za
ORCID iD: [1]0000-0002-9504-4705 [2]0000-0001-6582-8157

ABSTRACT

During fabrication of modified 9Cr–1Mo steels, δ-ferrite formed in the weld metal and heat-affected zone may not transform completely to austenite during subsequent cooling. The influence of changes in weld metal composition on δ-ferrite content was investigated using weld pads produced using basic coated P91 electrodes from four different manufacturers. The weld pads were designated Electrode 1, 2, 3, and 4 according to the different manufacturers. Electrode 1 and 3 fully complied with the EN ISO 3580-A CrMo91 specification. Electrode 2 had very low nickel and high niobium contents and Electrode 4 had carbon content above the maximum allowable limit. Thermo-Calc results showed that the temperature range over which a mixture of δ-ferrite and austenite is stable (the $Ae_4 - Ae_3$ temperature range) was smaller by more than 100 °C for Electrode 2 when compared with those of the other three electrodes. The limited ($Ae_4 - Ae_3$) temperature range, high ferrite factor, and chromium−nickel balance value of Electrode 2 were associated with an increase in the δ-ferrite content of the weld metal. Metallography results confirmed a significant amount of δ-ferrite in the as-welded microstructure of Electrode 2. Thermo-Calc estimates for the amount of δ-ferrite at high temperatures were supplemented by experimental anneal heat treatment on the weld metal. High-temperature anneal heat-treatments were carried out at 1320 °C and 1420 °C. The amount of δ-ferrite in the high-temperature annealed and quenched samples was significantly lesser than predicted by Thermo-Calc property diagrams.

Keywords: 9Cr–1Mo (P91) electrode, delta ferrite, Thermo-Calc, high–temperature anneal

1. INTRODUCTION

P91 steel is a ferritic–martensitic steel in the 9%–12%Cr family that is modified by nitrogen, niobium, and vanadium additions. Modified 9Cr–1Mo (P91) steel has attractive properties, such as high creep rupture strength, good resistance to stress corrosion cracking, low thermal expansion coefficient, and high thermal conductivity, which makes this steel suited for long-term elevated-temperature application in power-generating plants [1]. For adequate performance of modified 9Cr–1Mo steels, the alloy design and thermo-mechanical processes during manufacturing should be such that a fully martensitic microstructure is achieved that is free from delta (δ) ferrite. The presence of δ-ferrite, even in small quantities, in the final microstructure has a detrimental effect on mechanical properties [2], especially creep rupture strength in long-term high-temperature applications [3]. Production of P91 base metal always includes austenitisation at temperatures of 1040–1150 °C to dissolve any retained δ-ferrite, followed by air cooling and tempering [4]. During fabrication, austenitisation is not a feasible post-weld heat treatment, so δ-ferrite formed in the weld and heat-affected zone may not transform completely to austenite during subsequent cooling. It is under these circumstances that retained δ-ferrite is often observed in the weld−metal final microstructure [5].

A strict balance between austenite- and ferrite-forming elements in P91 is necessary to ensure that no δ-ferrite is present in the weld metal. The retention of δ-ferrite in the weld metal is often predicted from the chemical composition using modifications of the Schaeffler, Schneider, Kaltenhauser, and Newhouse empirical formulas [6]. To obtain weld metals free from δ-ferrite, Onoro [7] stated that a Schneider chromium equivalent (Cr_{eq}) value lower than 13.5 and the difference between the chromium (Cr_{eq}) and nickel equivalents (Ni_{eq}), referred to as the ferrite factor (FF) lower than 8 is necessary. The Schneider formulas are as follows:

$$Cr_{eq} = Cr + 2Si + 1.5Mo + 5V + 1.75Nb + 0.75W \quad (1)$$

$$Ni_{eq} = Ni + 0.5Mn + 30C + 25N + 0.3Cu \quad (2)$$

Honda et al. [8] have reported that having Cr_{eq} and Ni_{eq} lower than the proposed limits does not always prevent the formation of δ-ferrite. Roberts et al. [9] suggested using the chromium–nickel balance (CNB), given by Equation 3:

$$CNB = Cr + 6Si + 4Mo + 1.5W + 5Nb + 9Ti + 11V + 12Al - 40C - 30N - 2Mn - 4Ni - 1Cu \quad (3)$$

Swindeman et al. [4] reported that if the CNB is less than 10, δ-ferrite is not usually present; for CNB above 12, significant quantities of δ-ferrite are observed.

In the current investigation, shielded metal–arc welding was performed using four coated P91 electrodes from different manufacturers. The main objective was to investigate the influence of compositional differences on δ-ferrite content in the weld metal and δ-ferrite/austenite (δ/γ) phase-transformation temperatures. Thermo-Calc modelling results for the amount of δ-ferrite at high temperatures were supplemented by experimental anneal heat treatment on the weld metal. The annealing was performed at a temperature range in the equilibrium phase diagram where both δ-ferrite and austenite are stable. Additionally, the annealing experiments also enabled us to study the kinetics of delta-ferrite/austenite transformation during cooling.

2. EXPERIMENTAL PROCEDURE

A P91 sectioned pipe with a thickness of 40 mm was used as the base metal for the weld pads. Figure 1 (a) shows a photograph of the sectioned weld pad. A stereoscope image of the weld pad cross-section is shown in Fig. 1(b). Two weld pads were prepared from each electrode, each with a size of 20 mm × 25 mm × 70 mm. One weld pad was deposited with the base metal preheated to 200 °C and the inter-pass temperature maintained at a minimum value of 200 °C during welding; the other weld pad received no preheating.

(a) 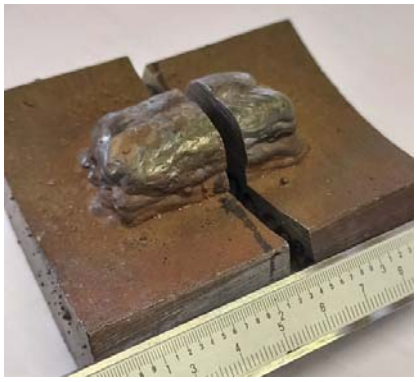 (b) 

Fig. 1 (a) A photograph of a sectioned weld pad on the P91 base metal. (b) Stereoscope images of the weld pad cross-section at 10X magnification.

Table 1 shows typical weld metal compositions of the electrodes (designated Electrodes 1, 2, 3, and 4), as supplied by the respective manufacturers.

Table 1. Typical analysis of weld metal (mass%), as supplied by electrode manufacturers.

	C	Mn	Cr	Si	Mo	V	Nb	Ni
EN ISO 3580-A CrMo91 Standard	0.06–0.12	0.4–1.5	8.0–10.5	0.6 max	0.8–1.2	0.15–0.30	0.03–0.10	0.4–1.0
Electrode 1	0.10	0.6	8.5	0.2	1.0	0.20	0.06	0.5
Electrode 2	0.09	1.0	9.0	0.2	1.0	0.22	0.07	-
Electrode 3	0.10	0.7	9.0	0.4	1.0	0.20	0.06	0.7
Electrode 4	0.09	0.6	9.0	0.2	1.1	0.20	0.05	0.8

P91 welds usually receive a temper treatment at a minimum temperature of 730 °C for 2 h to achieve optimum mechanical properties, but, in the current investigation, the pads were analysed in the as-welded condition.

Table 2 presents the chemical compositions of the four weld pads, performed on the last bead deposited using the optical emission spectrograph (OES) technique. Electrode 1 and 3 fully complied with the EN ISO 3580-A CrMo91 specification. Electrode 2 had very low nickel and high niobium contents and Electrode 4 had carbon content above the maximum allowable limit.

Table 2. Average chemical composition (mass%) of weld metal pads (EN ISO 3580-A CrMo91).

	C	Mn	Cr	Si	Mo	V	Nb	N	Ni	Al
EN ISO 3580-A CrMo91 Standard	0.06–0.12	0.4–1.5	8.0–10.5	0.6 max	0.8–1.2	0.15–0.30	0.03–0.10	0.02–0.07	0.4–1.0	–
P91 Electrode 1	0.12	0.58	9.31	0.21	1.05	0.22	0.076	0.043	0.44	≤0.005
P91 Electrode 2	0.10	0.98	9.92	0.43	1.13	0.24	0.144	0.038	0.05	≤0.005
P91 Electrode 3	0.12	0.74	9.34	0.36	1.01	0.27	0.065	0.031	0.68	≤0.005
P91 Electrode 4	0.15	0.52	10.30	0.22	1.06	0.22	0.071	0.027	0.74	≤0.005

Thermo-Calc version 2019b thermodynamic software was used with the TCFE7 database to perform one-axis equilibrium calculations based on the actual chemical compositions of the welds shown in Table 2. The equilibrium transformation sequence and temperatures were hence determined. An equilibrium phase diagram was constructed for the P91 composition with a range of mass percentage chromium. Individual phase diagrams with elemental range of carbon, nickel and niobium were also constructed because they fall outside the composition specification limits in the Electrode 2 and 4.

High-temperature anneal heat-treatments were carried out at 1320 °C and 1420 °C with soaking times of 60 min followed by a subsequent water quench. The heat-treated samples with dimensions of 10x10x5 mm were sectioned from the weld pads. The annealing was done on a vertical tube furnace under Argon gas atmosphere with an external thermocouple inserted to verify the temperatures during heat treatment.

Optical metallography and scanning electron microscopy with energy-dispersive X-ray spectroscopy (SEM–EDS) were carried out on the weld pads in both the as-welded and high-temperature annealed conditions. The phase fraction calculation of the microstructures was performed through ImageJ area fraction measurement. Electron backscatter diffraction (EBSD) analysis was performed on the as-welded samples only, using a Joel JSM instrument at an accelerating voltage of 20 kV and working distance of 10 mm.

3. RESULTS AND DISCUSSION

The as-welded optical microstructure of Electrode 2, shown in Fig. 2(a), indicated about 13% volume fraction of δ-ferrite in the weld metal of the last-deposited beads. In contrast, that of Electrode 3, shown in Fig. 2(b), showed martensitic matrix with small amounts (0.4 %) of δ-ferrite retained in the fusion line between the weld beads. The weld metals of Electrodes 1 and 4 were fully martensitic. The use of preheating (200 °C) did not change the amount of δ-ferrite in Electrode 2 weld metal.

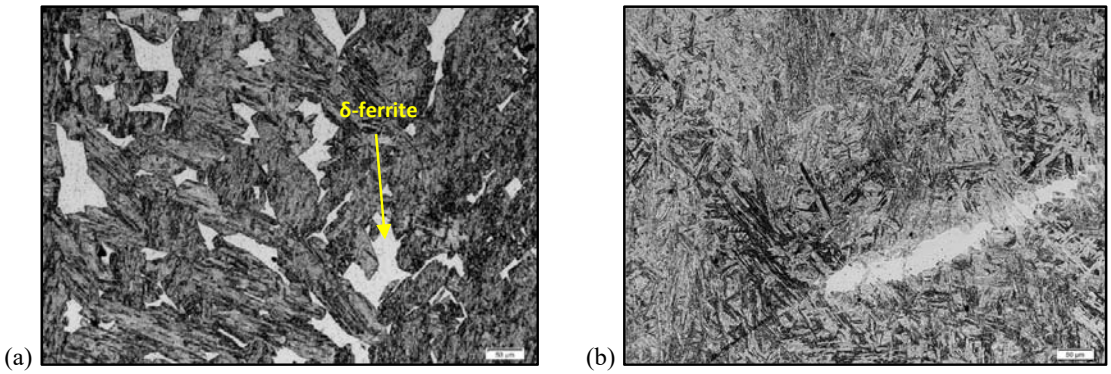

Fig. 2 Optical images of as-welded microstructures of (a) Electrode 2, showing a martensitic matrix with δ-ferrite in the last-deposited beads and (b) Electrode 3, showing martensitic matrix with δ-ferrite in the fusion line between the weld beads. 200× magnification

An optical image of the Electrode 2 weld annealed at 1320 °C (Fig. 3(a)) showed that the microstructure consisted of martensitic matrix with 23% δ-ferrite. Electrode 3, shown in Fig. 3(b), consisted of a martensitic matrix with about 2% δ-ferrite. No δ-ferrite was observed in Electrodes 1 and 4 weld metals that were heat-treated at 1320 °C.

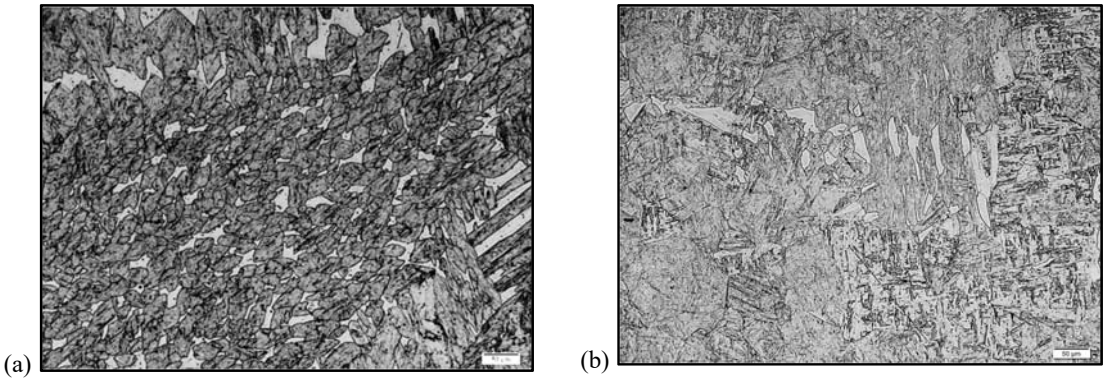

Fig. 3 Optical microstructure images of welds annealed at 1320 °C for 1 h. (a) Electrode 2, comprising of a martensitic matrix with 23% δ-ferrite and (b) Electrode 3, comprising a martensitic matrix with about 2% δ-ferrite. 200× magnification.

The volume fraction of δ-ferrite observed in Electrode 2, shown in Fig. 4(a) exceeded 70% when heat-treated at 1420 °C. Electrodes 1, 3, and 4 welds that were heat-treated at 1420 °C showed a martensitic matrix with 16%–19% δ-ferrite shown in Fig. 4(b).

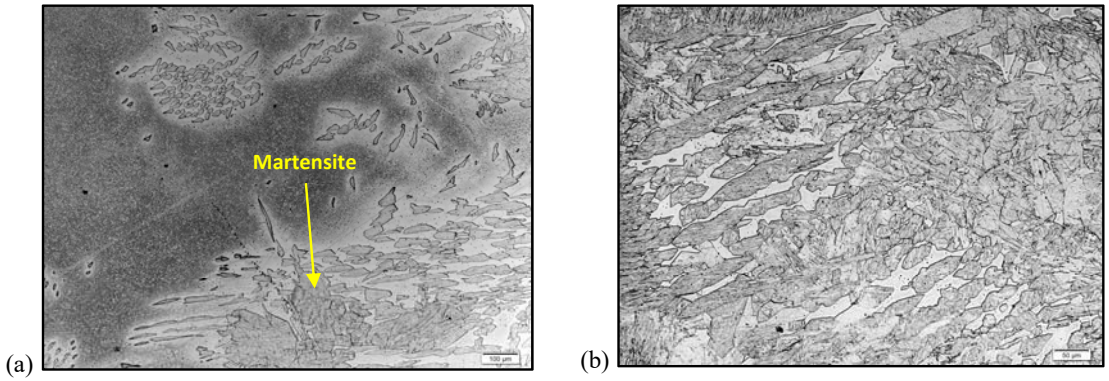

Fig. 4 Optical microstructure images of welds annealed at 1420 °C for 1 h. (a) Electrode 2, comprising a 72% δ-ferrite matrix with martensite at 100× magnification. and (b) Electrode 3, comprising a martensitic matrix with about 19% δ-ferrite at 200× magnification.

EBSD was applied to determine if any austenite phase was present in the as-welded microstructures of the four electrodes. Figure 5(a) presents an EBSD phase map that shows the presence of only a body-centred cubic (bcc) crystal structure; no evidence of austenite was observed in the as-welded samples. Differentiating between martensite and δ-ferrite was difficult because of the similarities in the crystallographic structures of the two phases. EDS was performed to determine whether any partitioning of elements between the phases or segregation along the phase boundaries could be detected. There was no evidence of any chemical segregation between the δ-ferrite and martensitic phases (Figs. 5(b, c)). A difference in carbon concentration between the δ-ferrite and martensite phase may exist but the EDS detector was not sensitive enough to detect differences at the concentrations present in the welds. The green and brown images in Fig. 5(b) represents elemental mapping scans for oxygen and manganese respectively. The dark region in the oxygen map is a shadowing effect from the surface topology which is an artefact of the acquisition process. Figure 5(c) shows chromium and nickel EDS line scans represented by the pink and blue scans respectively.

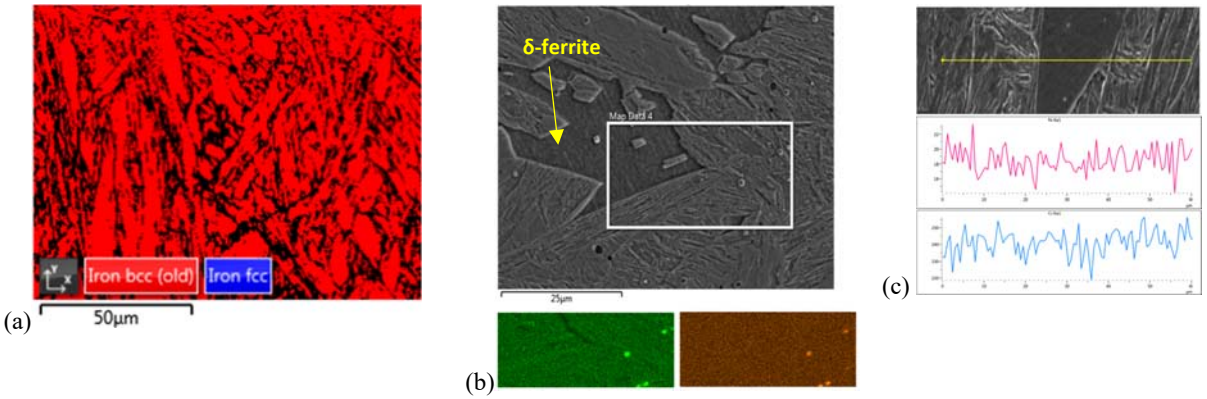

Fig. 5 (a) EBSD phase map (red: martensite and δ-ferrite) of Electrode 2 weld showing the presence of only iron bcc phases. (b) Elemental mapping scan of between δ-ferrite and martensite phases showing no segregation, although some inclusions are observed. (c) EDS line scan analysis, showing no evidence of segregation.

Based on the chemical compositions in Table 2, Schneider empirical formulae and the CNB were used to predict the presence of δ-ferrite in the final weld metal [4]. The results are presented in Table 3.

Table 3. Ferrite factor ($Cr_{eq} - Ni_{eq}$) and chromium−nickel balance (CNB) to predict δ-ferrite retention.

	Cr_{eq} (< 13.5)	**Ni_{eq}**	**FF (< 8)**	**CNB (< 12)**
P91 Electrode 1	12.5	5.4	7.1	8.6
P91 Electrode 2	13.9	4.5	9.4	13.1
P91 Electrode 3	13.0	5.4	7.6	9.0
P91 Electrode 4	13.6	6.2	7.4	7.9

Electrode 2 had the most indicators of δ-ferrite retention in the weld metal due to its high FF and CNB values. The weld metal from Electrode 4 had a marginally high chromium equivalent, but no δ-ferrite was observed in the weld metals because of the balancing effect of the nickel equivalent.

Figure 6 shows P91 equilibrium phase diagrams constructed using Thermo-Calc software, where Fig. 6(a) shows the variation in chromium content between 5 and 15 mass%, Fig. 6(b) shows the range of carbon content between 0 and 0.25 mass%, Fig. 6(c) shows a content range of nickel between 0 to 2 mass% and Fig. 6(d) is a 0 to 0.2 mass% of niobium content range. Chromium is the main alloying element in P91 steel because of its influence in both oxidation resistance and creep strength and is a strong ferrite former. The equilibrium phase diagrams with chromium variation demonstrates clearly the influence of chromium on transformation temperatures and on restricting the austenite phase field. Higher chromium content leads to increased chance of delta ferrite presence in the final weld metal. Carbon, nickel and niobium were outside the composition specification limits as shown in table 2 and thus it was important to highlight the extent of their influence on the Ae_4 and Ae_3 transformation temperatures. The red lines on the diagrams in Fig. 6 indicate the weld metal element's average specification range. The temperatures of the high-temperature anneal heat-treatment are indicated by the blue dots in Fig. 6. Austenite and δ-ferrite are both stable at the annealing temperature.

The equilibrium transformation temperatures are defined as follows (on heating):

Ae_1: onset of austenite formation;
Ae_3: fully austenitic phase is achieved;
Ae_4: onset of δ-ferrite formation from austenite;
Ae_5: completion of austenite to δ-ferrite transformation

In comparing the phase diagrams of Fig. 6, the effect on transformation temperature of the elements is evident. Carbon and nickel are austenite formers and enlarges the ($Ae_4 - Ae_3$) temperature range which reduces the tendency for δ-ferrite retention. The strong effect of nickel on the Ae_1 temperature is evident in Fig. 6(c). Niobium is a ferrite former but shows minimal effect on the transformation temperatures as seen in Fig. 6(d); it is manly added as a carbo-nitride former. This highlights the importance of achieving a good balance between ferrite- and austenite-forming elements in P91 alloys because of their influence in the ($Ae_4 - Ae_3$) temperature range.

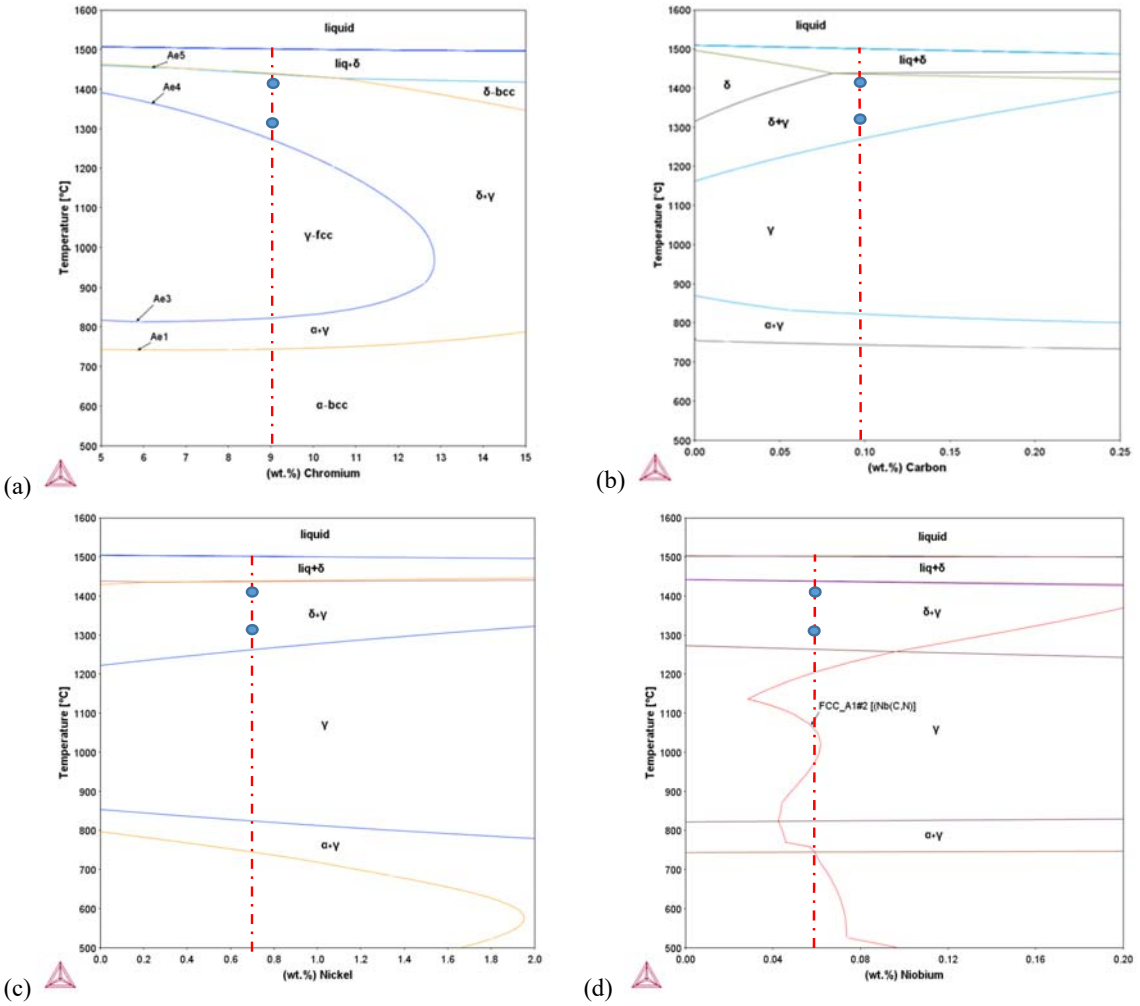

Fig. 6 P91 compositional phase diagrams showing (a) 5 to 15 mass % chromium, (b) 0 to 0.25 mass % carbon, (c) 0 to 2 mass % nickel and (d) 0 to 0.2 mass % niobium.

The Thermo-Calc equilibrium property diagrams shown in Fig. 7 revealed different phase-transformation sequences that takes place during cooling, depending on the composition of the weld deposit:

$$\text{Liquid} \rightarrow \text{liquid} + \delta \rightarrow \text{liquid} + \delta + \gamma \rightarrow \delta + \gamma \rightarrow \gamma \qquad \text{(Electrode 1, 3 and 4)}$$

$$\text{Liquid} \rightarrow \text{liquid} + \delta \rightarrow \delta \rightarrow \delta + \gamma \rightarrow \gamma \qquad \text{(Electrode 2)}$$

The thermodynamic property diagram for Electrode 4, shown in Fig. 7(a), was very similar to those of Electrodes 1 and 3. The transformation temperatures and behaviour of Electrode 2, shown in Fig. 7(b), was slightly different, in that solidification was almost complete before the onset of austenite formation; Electrodes 1, 3, and 4 still had a significant amount of liquid when austenite started forming.

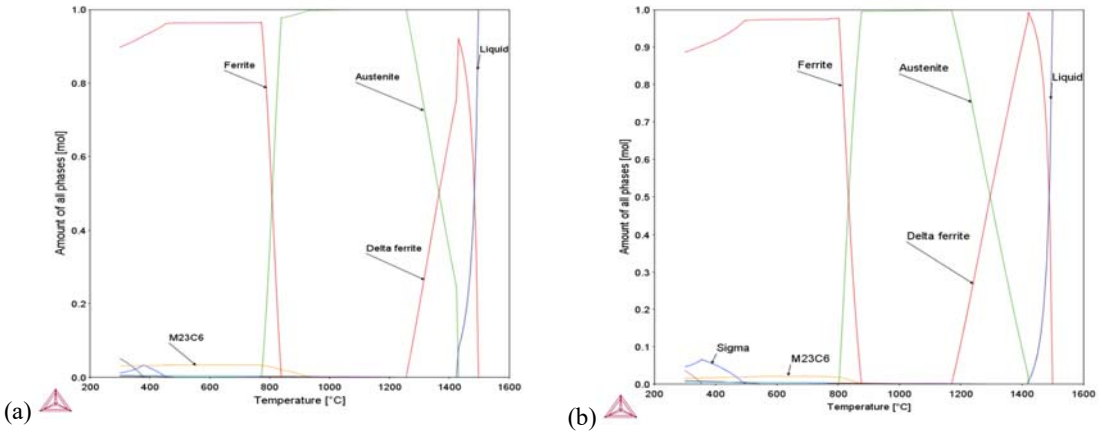

Fig. 7 Property diagrams for (a) Electrode 4 and (b) Electrode 2 weld metals showing the mole fraction of phases as a function of temperature.

Arivazhagan and Kamaraj [6] stated that the chance of δ-ferrite retention in the weld increases with a lower value of ($Ae_4 - Ae_3$). A larger ($Ae_4 - Ae_3$) value means that austenite is stable over a wider range of temperature and that δ-ferrite has more time to transform to austenite during cooling. The equilibrium transformation temperatures determined from the property diagrams are listed in Table 4. Electrodes 1, 3, and 4 weld metals had ($Ae_4 - Ae_3$) temperature ranges between 417 and 434 °C, which are more than 100 °C larger than the corresponding temperature range for Electrode 2 weld metal.

Table 4. Thermo-Calc equilibrium transformation temperature (°C)

	Ae_1	**Ae_3**	**Ae_4**	**Ae_5**	**Solidus Temp**	**($Ae_4 - Ae_3$)**
P91 Electrode 1	796	840	1271	1439	1434	431
P91 Electrode 2	802	876	1170	1420	1430	294
P91 Electrode 3	764	836	1270	1435	1431	434
P91 Electrode 4	773	839	1256	1431	1424	417

Table 5 summarises the results from the Thermo-Calc calculations and ferrite-prediction empirical formulas compared with the measured phase fraction of δ-ferrite in both the as-welded and high-temperature annealed samples. Electrode 2 had the smallest ($Ae_4 - Ae_3$) temperature range and high FF and CNB values. These characteristics resulted in a significant amount of δ-ferrite in the weld metal when compared with other electrodes.

Table 5. Measured amounts of δ-ferrite in the as-welded and annealed (HT) compared to thermo-calc predicted results

	($Ae_4 - Ae_3$)	**FF**	**CNB**	**Measured % δ-ferrite**			**Thermo-Calc predicted % δ-ferrite**	
				As-welded	**HT @ 1320 °C**	**HT @ 1420 °C**	**1320 °C**	**1420 °C**
Electrode 1	431	7.1	8.6	–	–	18	25	76
Electrode 2	294	9.4	13.1	13	23	72	60	98
Electrode 3	434	7.6	9.0	0.4	2	19	27	78
Electrode 4	417	7.4	7.9	–	–	16	29	74

(‗) means that the microstructure was fully martensitic:

A small amount of δ-ferrite was observed on the as-welded microstructure of Electrode 3 even though the ferrite-predicting empirical formulae values were within the recommended limits. The chromium equivalent (Cr_{eq}) was slightly above the recommended limit and the carbon content was above the specification limit for Electrode 4 but the microstructure was fully martensitic. The empirical formulas (FF and CNB) are not always accurate in predicting the presence of delta ferrite in the final weld metal.

The amount of δ-ferrite observed in the annealed welds was significantly lower than predicted by the Thermo-Calc property diagrams under equilibrium conditions. This may indicate that even with a very fast cooling rate, it is difficult to completely supress the δ-ferrite to austenite transformation.

4. CONCLUSIONS

Four commercial P91 electrodes were compared with respect to δ-ferrite content in the as-welded and high-temperature annealed conditions. Electrodes 1, 3, and 4 weld metals had ($Ae_4 - Ae_3$) temperature ranges exceeding 400 °C, which was more than 100 °C larger than that of Electrode 2 weld metal, which contained a significant amount of δ-ferrite in the final microstructure. The lack of nickel, which is an austenite stabiliser, in the Electrode 2 composition highlights the importance of a strict balance between austenite- and ferrite-forming elements in preventing the presence of δ-ferrite. Manufacturers' weld metal compositions should target the EN ISO 3580-A CrMo91 or similar standard to reduce the risk of δ-ferrite retention. As observed in the annealed weld-metal microstructures, the amount of δ-ferrite was significantly lower than predicted by Thermo-Calc property diagrams. Determining the high-temperature structure probably requires much higher cooling rates than can be achieved by water quenching.

5. DECLARATIONS

Funding: Southern African Institute of Welding

6. CONFLICT OF INTEREST

The authors declare that they have no conflict of interest.

7. REFERENCES

1. Pandey, C., Mahapatra, M.M., Kumar, P. and Saini, N., 2018. Some studies on P91 steel and their weldments. *Journal of Alloys and Compounds*, *743*, pp.332-364..
2. Arivazhagan, B. and M. Kamaraj (2013). "A study on influence of D-ferrite phase on toughness of P91 steel welds." White Paper, Steel-Grips. Com: 19-24.
3. Liu, X. Y. and T. Fujita (1989). "Effect of chromium content on creep rupture properties of a high chromium ferritic heat resisting steel." *ISIJ INTERNATIONAL* **29**(8): 680-686.
4. Swindeman, R.W., Santella, M.L., Maziasz, P.J., Roberts, B.W. and Coleman, K., 2004. Issues in replacing Cr–Mo steels and stainless steels with 9Cr–1Mo–V steel. *International Journal of Pressure Vessels and Piping*, *81*(6), pp.507-512.
5. Pandey, C., Giri, A. and Mahapatra, M.M., 2016. Evolution of phases in P91 steel in various heat treatment conditions and their effect on microstructure stability and mechanical properties. *Materials Science and Engineering: A*, *664*, pp.58-74.
6. Arivazhagan, B., Srinivasan, G., Albert, S.K. and Bhaduri, A.K., 2011. A study on influence of heat input variation on microstructure of reduced activation ferritic martensitic steel weld metal produced by GTAW process. *Fusion engineering and design*, *86*(2-3), pp.192-197.
7. Onoro, J., 2006. Martensite microstructure of 9–12% Cr steels weld metals. *Journal of Materials Processing Technology, 180*(1-3), pp.137-142.
8. Honda, T., Kusano, T., Osada, T., Hirano, K. and Takemoto, K., 1998. Development of 9Cr-2W cast steel for the valves in elevated temperature fossil power plants. In *Advanced heat resistant steels for power generation (San Sebastian, 27-29 April 1998, preprints)*.
9. Roberts BW, Swindeman RW, Maziasz PJ, Wright IG. TVA experience in the application of 9Cr–1Mo–0.2V–Cb (Grade 91) steel. *Paper Presented at the EPRI Conference on 9Cr Materials Fabrication and Joining Technologies*, July 10–11, Myrtle Beach, South Carolina, USA; 2001.

10. Wang, Y., Mayer, K.H., Scholz, A., Berger, C., Chilukuru, H., Durst, K. and Blum, W., 2009. Development of new 11% Cr heat resistant ferritic steels with enhanced creep resistance for steam power plants with operating steam temperatures up to 650 C. Materials Science and Engineering: A, 510, pp.180-184.